

Essential Role of Thiols in Maintaining Stable Catecholato-Iron Complexes in Condensed Materials

Hyungbin Kim, Jinhoon Lee, Yuri Hong, Chanoong Lim, Dong Woog Lee,* Dongyeop X. Oh,* J. Herbert Waite,* and Dong Soo Hwang*



Cite This: *Chem. Mater.* 2022, 34, 5074–5083



Read Online

ACCESS |



Metrics & More

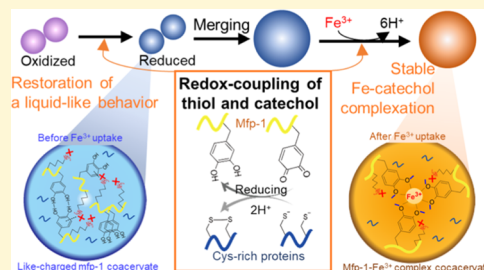


Article Recommendations



Supporting Information

ABSTRACT: The load-bearing proteins in mussel holdfasts rely on condensed *tris*-catecholato- Fe^{3+} coordination complexes for their toughness and shock-absorbing properties, and this feature has been successfully translated into synthetic materials with short-term high-performance properties. However, oxidation of catecholic DOPA (3,4-dihydroxyphenylalanine) remains a critical impediment to achieving materials with longer-lasting performance. Here, following the natural mussel pathway for protein processing, we explore how DOPA oxidation impacts coacervation of mussel foot protein-1 (mfp-1) and its capacity for phase-specific metal uptake in vitro. Without metal, DOPA oxidation changed the rheological properties (i.e., viscosity, loss, and storage moduli) of mfp-1 coacervate droplets. However, oxidation-dependent changes were recovered with dithiothreitol (DTT), completely restoring the behavior of mfp-1 coacervates prior to oxidation. With metal, mfp-1 coacervates exhibited gel-like behavior with high viscosity and cohesive forces by forming recognizable *bis*- and *tris*-catecholato- Fe complexes, linked to increased energy dissipation and toughness of byssus. These results indicate that Fe^{3+} -mediated conversion of liquid–liquid phase-separated polymers into metal-coordinated networks is thorough and rapid, and DTT effectively maintains redox integrity. Our study provides much-needed improvements for processing catechol-functionalized polymers into high-performance materials.



INTRODUCTION

Mussels are permanently sessile and rely on a multithread holdfast called byssus for secure attachment. Byssal threads are natural load-bearing consumer products with a manufacturing time of ~ 5 min and a useful lifetime of ~ 1 year.¹ There is no question that byssal threads and their uncanny combination of strength, toughness, self-healing, and shock-absorbing properties are critical to mussel survival in turbulent high-energy surf areas.^{2–4} Much attention has been devoted to mimicking the contributions of various byssal proteins. Even more important is investigating how specific molecular structures and processing strategies endow byssus with its functional properties.

A careful dissection of individual byssal threads has revealed distinct architectural compartments, namely, the core, cuticle, and plaque, which work in concert but face rather different functional challenges.⁵ The cuticle is a 1–5 μm thick abrasion-resistant coating covering the core and plaque (Figure 1A).^{6,7} Although the least conspicuous compartment, the cuticle has drawn as much attention as the other two.

3,4-Dihydroxyphenyl-L-alanine (DOPA), which is modified from tyrosine, plays an essential role in reinforcing mechanical properties of biomaterials through H-bonding, cross-linking, and metal coordination in living organisms (e.g., squid beak, insect cuticle, mussel byssus, and polychaete jaws).^{8–10} In the mussel byssal cuticle, especially, the high contents of DOPA

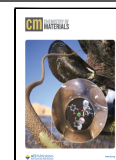
and Fe^{3+} probably account for its mechanical properties.^{11,12} In *Mytilus* species, most of the DOPA comes from mussel foot protein-1 (mfp-1), that is, intrinsically disordered and consists of 60 or more tandem repeats of a decapeptide Ala-Lys-Pro-Ser-DOPA–DHP-Hyp-Thr-DOPA-Lys (Hyp is 4-trans-hydroxy-L-proline and DHP is dihydroxy-L-proline) (Figure 1B).^{13–15} Mfp-1 is localized together with Fe^{3+} and V^{4+} in the discontinuous granules (0.5 μm diameter) of a biphasic cuticle structure.^{3,6} Therefore, based on resonance Raman microscopy, DOPA and Fe^{3+} interact as *bis*- and *tris*-catecholato-iron complexes. Efforts to exploit this kind of chemistry in engineered tough self-healing synthetic hydrogels and epoxies and biomedical applications have generated much attention,^{16–21} but oxidative instability of DOPA remains a limiting impediment.

As nature's DOPA-containing materials seem much less susceptible to DOPA instability,^{22,23} insights about natural strategies to counter and/or mitigate oxidation have a high fundamental and practical value. Three mechanistic insights

Received: February 8, 2022

Revised: May 5, 2022

Published: May 19, 2022



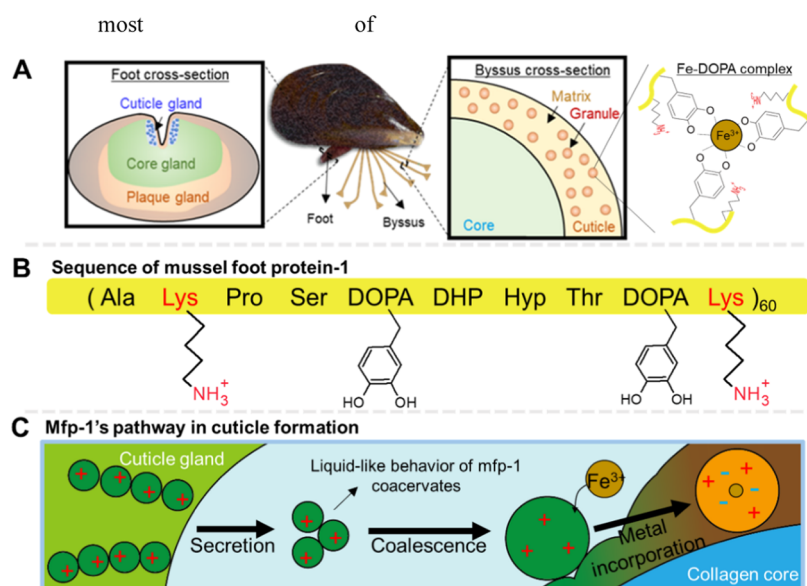


Figure 1. Overview of the cuticle formation of mussel byssus. (A) Illustration of the foot and byssus in cross section, and Fe-DOPA complex in the granule of byssus. (B) Consensus sequence of mussel foot protein-1 (mfp-1). (C) Mfp-1's pathway in cuticle formation.

have emerged from experiments on DOPA-containing proteins: (1) in mussel adhesive proteins, interfacial DOPA oxidation is reduced by thiols in mfp-6;^{24,25} (2) colocalization of mfp-6 and mfp-3 in coacervate droplets appears to insulate them indefinitely from oxidants;²⁶ and (3) a similar relationship between different proteins has been proposed for redox at the interface between the cuticle and core in byssus.²⁷ Cys-rich proteins such as mfp-16 to mfp-18, for example, are considered to be key reducing agents in the byssal cuticle.^{28,29} As reducing agents, the thiols of Cys-rich proteins are able to recover DOPA from DOPAquinone by donating $2e^-$ and $2H^+$ /quinone. By this action, thiols are unlikely to alter the mfp-1 structure because mfp-1 is an intrinsically disordered protein (IDP) and lacks cysteine.

The current view of mfp-1's pathway in cuticle formation is the following (Figure 1C): first, mfp-1 condenses into polymer-rich dense phase by the known cation- π interaction between positively charged lysine and DOPA called liquid-liquid phase separation or coacervation. The mfp-1 coacervates are stockpiled in secretory vesicles of the cuticle gland and then are secreted into longitudinal ducts, where they undergo coalescence. Metals such as iron and/or vanadium are introduced by catecholic carriers and transferred to mfp-1 coacervates just before the complex fluid emerges into the ventral groove, and, finally, the metal-containing fluid is applied as a film over the collagen core of each nascent thread.^{29,30}

The aims of the present study were to determine whether (1) the mfp-1 coacervates serve as a sink for metal ion uptake and metal-mediated gelation; (2) damage to mfp-1 by DOPA oxidation occurs in all phases of the protein; (3) DOPA oxidation has an effect on the rheological properties of mfp-1 phases; (4) thiols such as dithiothreitol (DTT), a low molecular weight mimic of Cys-rich proteins, prevent DOPA oxidation by maintaining a reducing redox poise; and (5) at the concentrations used, DTT interferes or not with catecholato-iron coordination.

EXPERIMENTAL SECTION

Purification of Mussel Foot Protein-1 and Recombinant Mfp-1. Purification and extraction of mfp-1 were described in the previous studies.^{13,31} Mussel (*Mytilus edulis*) feet were obtained from NorthEast Transport (Walpole, ME). Mussel feet were harvested and frozen at -80°C before protein extraction. The phenol glands of mussel feet were crushed in liquid nitrogen using a homogenizer and ground with a tissue grinder. Crude mfp-1 was extracted using an extraction buffer (5% (v/v) acetic acid, 0.1 M EDTA, 0.1 mM leupeptin, and 0.1 mM pepstatin). The supernatant was collected after centrifugation at 14,000 rpm at 4°C for 30 min. Mfp-1 was further purified by the addition of 1.4% (v/v) perchloric acid. The soluble part containing mfp-1 was dialyzed with 5% acetic acid with a molecular weight cutoff of 10 kDa to remove small components, while the insoluble part was removed. The final dialyzed solution was concentrated by freeze-drying and stored at -80°C for further purification. A pure mfp-1 sample was obtained after further purification steps using a gel permeation column (Shodex KW 803) and C8 (RP-300, PerkinElmer, Waltham, MA) reversed-phase high-performance liquid chromatography (HPLC). The dried sample was resuspended in 5% acetic acid and injected into a gel permeable column (Shodex KW 803). The sample was monitored at 230/280 nm and collected with 5% acetic acid at 1 mL/min at 22°C . Then, the collected samples in 5% acetic acid were separated by C8-HPLC using an acetonitrile gradient in water with 0.1% trifluoroacetic acid. Pure mfp-1 was eluted at approximately 40% acetonitrile (Figure S1), and the fractions were freeze-dried and stored at -80°C . To ensure freshness, mfp-1 was used within a week of purification. Oxidized mfp-1 was prepared by dissolving the freeze-dried mfp-1 in the sodium acetate buffer, pH 5.5, for 10 h.

Purification of the recombinant mfp-1 (Rmfp-1) was described in the previous studies.^{32,33} Briefly, *E. coli* containing a plasmid to produce Rmfp-1 (12 repetitions of the mfp-1 decapeptide) was cultured in LB medium at 37°C , 250 rpm, and 1 mM isopropyl- β -D-1-thiogalactopyranoside (IPTG) was added when the optical density at 600 nm of the culture reached 0.3. Five hours after IPTG induction, the cells were harvested by centrifugation, and the harvested cells were disrupted by sonication and lysozyme treatment. Inclusion bodies (IBs) of the disrupted cells were collected, and Rmfp-1 inside the IB was extracted 10 (v/v)% acetic acid and injected into the gel permeable column and then C8-HPLC column as same as the purification of mfp-1. Pure Rmfp-1 was eluted at approximately 50%

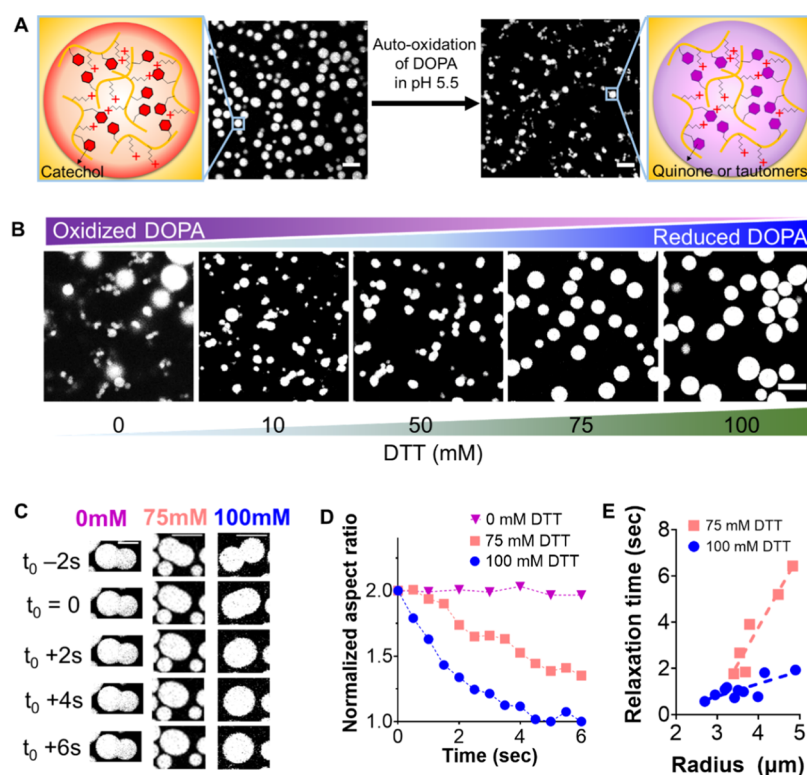


Figure 2. Effect of thiols on coalescences of the like-charged mfp-1 coacervate droplets. (A) Observation of the like-charged mfp-1 coacervates under a confocal microscope. Red hexagons (left): catechol moiety (DOPA). Purple hexagons (right): DOPAquinone or its tautomers after auto-oxidation. (B) Confocal images of the oxidized mfp-1 coacervates with various DTT concentrations. (C) Serial confocal images of the merging droplets at different DTT concentrations. (D) Aspect ratio (A) of the merging droplets at different DTT concentrations. $A = (L - W)/(L + W)$, where L is a long radius and W is a short radius. (E) Relaxation time (m) of the droplets depending on the radius. $A = 1 + \exp(-t/m)$, where t is time. Scale bar = 10 μm .

acetonitrile (Figure S1). The purity of both proteins was confirmed by SDS-PAGE gel, acid-urea gel (AU-Gel), and MALDI-TOF.

Preparation of Mfp-1 Coacervates. Mfp-1 concentration was calculated by Bradford assay; coacervation (1 mg/mL) was induced in 0.7 M NaCl and 0.1 M sodium acetate buffer (pH 5.5 or pH 7). To determine the reducing effect of DTT, mfp-1 containing oxidized DOPA tautomers such as dehydro-DOPA and quinone was phase-separated in 0.7 M NaCl with varying DTT concentrations. To explore metal incorporation into the mfp-1 coacervate, mfp-1-Fe³⁺ complex coacervates were formed by adding a small volume (below 0.01 volume) of FeCl₃ solution to the mfp-1 coacervate solution. The final FeCl₃ concentration was 400 μM .

Reducing Effect of DTT. Reduction of oxidized mfp-1 coacervates in the presence of DTT was observed by UV-vis spectroscopy and MALDI-TOF mass spectrometry. Absorbance changes in fresh and oxidized mfp-1 coacervates following 100 mM DTT addition were measured by UV-vis spectroscopy (Nanodrop2000, Thermo Scientific, Waltham, MA). Absorbances at 320–350 nm and 400 nm indicate dehydro-DOPA and DOPAquinone, respectively, according to previous studies.^{34,35} In addition, recovery of DOPAquinone to DOPA in the mfp-1 coacervates was detected by mass changes in mfp-1 using MALDI-TOF (Bruker, Billerica, MA). The oxidized mfp-1 coacervates formed at 0.7 M NaCl were reduced with 100 mM DTT at pH 5.5. The coacervate solution was desalted using Zip-tip (ZTC18S, Sigma, Saint Louis, MO), mixed with sinapinic acid (SA) solubilized in 0.1% TFA and 50% ACN, and spotted onto a steel MALDI plate.

Passive Microrheology. Red fluorescent beads (L3280, Sigma, Saint Louis, MO) with a diameter of 0.5 μm were prepared by coating with covalently bound poly(ethylene glycol) (PEG) to minimize the interaction between the beads and the protein. Mfp-1 was prepared by tagging fluorescein isothiocyanate (FITC) with green fluorescence. A small fraction (0.01 volume) of the beads was added to the coacervate

solution and gently mixed by pipetting. Then, the solution flowed into a custom-made chamber with a 100 μm spacer sandwiched between a glass and a coverslip. The mobility of the embedded beads ($n \geq 10$) into the coacervates was observed under a confocal microscope (FV3000, Olympus, Tokyo, Japan) equipped with a 60 \times objective. Serial images were acquired at constant intervals (0.5 or 1 s) for 5 min at 20 $^{\circ}\text{C}$. We calculated the mean squared displacement (MSD) of the embedded beads using MATLAB software (Mathworks, MA). To estimate the diffusion constant, D , we fit the form to $\text{MSD} \sim 4D\tau^{\alpha}$, where α is the diffusive exponent. The viscosity, η , of the coacervates was calculated when $\alpha \approx 1$ using the Stokes–Einstein equation, $D = k_{\text{B}}T/6\pi\eta a$, where k_{B} is the Boltzmann constant, $T = 295 \text{ K}$ is the temperature, and $a = 250 \text{ nm}$ is the bead radius. Dynamic shear moduli were obtained from the Laplace domain, $G'(s) = k_{\text{B}}T/\pi as$, where s is the Laplace frequency, which is calculated from the unilateral Laplace transform of $\langle \Delta r^2(t) \rangle$ using the generalized Stokes–Einstein equation.^{36,37}

Coalescence Experiments of Coacervates. The FITC tagged mfp-1 coacervate solution under different reducing conditions was prepared and added into a fluid chamber with a flat oil/water interface to minimize the friction between the coverslip surface and the coacervates during coalescence events. The surface of the bottom coverslip was coated using Sigmacote (SL2, Sigma, Saint Louis, MO), and the interface was stabilized with a PFPE-PEG-PFPE triblock copolymer surfactant (E2K0660, RAN Biotechnologies, Inc., Beverly, MA). Images of the coalescing coacervates were obtained using a confocal microscope with 60 \times objectives at 0.1 s intervals. The aspect ratio, A , was determined by calculating $A = (L - W)/(L + W)$, where L is a longer radius. And normalized aspect ratio ($1 + A/A_0$, where A_0 is the initial aspect ratio) was plotted with time (t). This aspect ratio was fitted to a function of the form $A = 1 + \exp(-t/m)$, where t is time and m is the relaxation time. We used a formula for the relaxation kinetics of a relaxed liquid droplet to estimate the interfacial tension³⁸

$$m \cong \frac{19\eta r}{20\sigma} \quad (1)$$

which shows the relaxation time, m , as a function of interfacial tension (σ), and the droplet radius (r), and viscosity (η) from eq 1.

Surface Force Apparatus (SFA) Experiments. The piezoelectric three-dimensional (3D) sensor/1D actuator attachment in SFA (Surforce LLC, Santa Barbara, CA) was used to measure the cohesive forces of mfp-1 coacervates. To prepare the coacervate cohesion substrate, freshly cleaved muscovite mica sheets (Grade #1, S&J Trading, Floral Park, NY) were glued onto two cylindrical disks using a UV glue (NOA81, Norland Products, Cranbury, NJ). Each disk was mounted on the upper 3D sensor/1D actuator, which is connected to strain gauges for converting vertical motion, and the lower main stage of the SFA chamber connected to a differential micrometer in a cylindrical cross geometry, respectively. Subsequently, 20 μ L of the coacervate solution was injected between the two mica surfaces. The displacement between two surfaces was controlled by the differential micrometer using a coarse micrometer with a constant speed (~ 2.2 mm/min) during loading and unloading. Figure 4a depicts a schematic of the SFA experimental setup and representative cohesive force profile. Briefly, two opposing surfaces were brought into contact (loading) to a targeted load (~ 300 mN) and followed by separation (unloading). The Fe-DOPA complexation in presence of DTT was also investigated by adding a small portion (0.2 μ L) of FeCl_3 solution in the coacervate. The final FeCl_3 concentration was 400 μ M.

The cohesive forces were translated from the measured voltage signals from the strain gauge, which is connected to a signal conditioning amplifier (2310B, Vishay, Malvern). Then, the acquired signals were recorded as loading/unloading profiles by a data acquisition system (Omniace RA2300, A&D, Tokyo, Japan). The strain gauge in the 3D sensor/1D actuator was calibrated by converting the corresponding load to voltage at the beginning of the experiment. All cohesive force measurements were conducted at 16 $^\circ\text{C}$ (below upper critical solution temperature, UCST) more than five times to confirm the reproducibility of measurements.

Observation of Temperature-Dependent Phase Behavior. The mfp-1 coacervate solution was freshly prepared in 0.7 M NaCl, 100 mM DTT, and 0.1 M sodium acetate buffer (pH 5.5) and added to a Hellma aluminum spacer (Z801240, Sigma, Saint Louis, MO). Then, 400 μ M FeCl_3 was added to form the mfp-1- Fe^{3+} complex coacervation. The turbidity of the coacervate solution was observed by heating and cooling ranging from 10 to 30 $^\circ\text{C}$ at a rate of 3 $^\circ\text{C}/\text{min}$ using a cyclic dichroism instrument (Jasco J-815, Jasco, MD).

Spectroscopic Analyses for Fe-DOPA Complexation. Raman spectra were acquired from mfp-1 coacervates, induced in a reducing high salt solution (0.7 M NaCl, 100 mM DTT in 0.1 M sodium acetate buffer (pH 5.5)), followed by the treatment with 400 μ M FeCl_3 or without FeCl_3 , using a confocal Raman microscope (LabRam Aramis, Horiba, Kyoto, Japan). A 50 \times objective and 514 nm laser (<1 mW power) were used. The acquisition time was <120 s. UV-vis absorbance of the mfp-1- Fe^{3+} coordination was observed at 500 nm for 3 h at 10 s intervals using UV-vis spectroscopy. Mfp-1 coacervates (1 mg/mL) in 0.1 M sodium acetate buffer (pH 5.5 or pH 7) were prepared, and DTT (0 or 100 mM) was added, followed by the treatment with 400 μ M FeCl_3 . The coacervate solution was treated with 1.2 mM NaIO_4 to induce DOPA oxidation (and subsequent quinone tautomerization).

RESULTS AND DISCUSSION

Coalescence Recovery of Mfp-1 Coacervate Droplets with Oxidized DOPA by Thiols. To prepare mfp-1 coacervate droplets for metal uptake, mfp-1 coacervation was induced by adding purified mfp-1 (1 mg/mL) to 0.7 M NaCl in acetate buffer (pH 5.5) whereupon it self-coacervates (Figures 2A and S2). Cation- π and π - π interactions presumably initiate the self-coacervation.³³ Although mfp-1 molecules typically repel one another given the high density of

positive charges, repulsion is suppressed by charge screening at 0.7 M salt. This phase separation of the positively charged droplets is referred to as a “like-charged mfp-1 coacervate”.

DOPA undergoes auto-oxidation to DOPAquinone or tautomers. Depending on pH and local chemistry, quinone formation can have two consequences that are not mutually exclusive: it can form covalent adducts via nucleophilic Michael additions with neighboring amino acids or it can lead to conformational changes, whereas quinone tautomers such as dehydro-DOPA and dehydro-DOPA-quinone transform the disordered chain into a more rigid (possibly less soluble) secondary structure, as previously reported.^{34,39,40} However, cuticle formation based on mfp-1 coacervation assumes that DOPA does not undergo oxidation within the like-charged mfp-1 coacervates.^{29,41} We observed the coacervate morphology to determine whether DOPA oxidation affects the formation of like-charged mfp-1 coacervates under a confocal microscope (Figure 2A). DOPA residues in mfp-1 were auto-oxidized by incubating in pH 5.5 buffer at 20 $^\circ\text{C}$; then, the high salt coacervation of mfp-1 was induced, and the droplet morphology was observed. Accordingly, fresh mfp-1 coacervate droplets were spherical, whereas coacervates from oxidized mfp-1 formed small irregular shapes. This morphological difference suggested that auto-oxidation of DOPA has rheological consequences for the coacervate.⁴²

Using mfp-1 with oxidized DOPA residues, we screened for DTT ability to reduce the oxidized DOPAquinone to DOPA by analyzing UV-vis spectroscopy and mass shifts using matrix-assisted laser desorption/ionization time-of-flight (MALDI-TOF) (Figure S3). The auto-oxidation of DOPA can be readily followed by UV-vis absorbance because absorbance at 280 nm is shifted to 320 nm and 400 nm, respectively, for dehydro-DOPA and DOPA-quinone.^{34,35} Before the addition of DTT, DOPA oxidation in mfp-1 was detectable in the UV-vis spectra (Figure S3A). Absorbance above 320 nm increased with the oxidation. The addition of 100 mM DTT to mfp-1 decreased absorbance above 350 nm. However, the absorbance at 320 nm was not decreased because oxidized DTT, which forms a disulfide-bonded six-membered ring, absorbs at 300 nm. Results suggest that DTT can be sacrificially oxidized with the reduction of the oxidized DOPA to DOPA. In addition, every DOPAquinone reduction to DOPA increases protein mass by +2 Da. For example, the mass of mfp-1 with the quinone was shifted by +180 Da following treatment with 100 mM DTT.

This shift was consistent with the reductive conversion of 90 quinones to DOPA residues (Figure S3B). These analyses confirmed that the redox activities of DTT and DOPA are coupled. Reduction with DTT would also prevent the occurrence of DOPA-quinone-mediated cross-linking for coalescence and metal uptake.

Following this, we observed the coalescences of the like-charged mfp-1 coacervate droplets in various DTT concentrations using confocal microscopy. The oxidized mfp-1 coacervate droplets, which were unable to coalesce without DTT, showed improved coalescence with increasing DTT concentration. In particular, the coacervate droplets became perfectly spherical above 100 mM DTT (Figure 2B). Normalized aspect ratios ($A/A_0 + 1$, where A_0 is the initial aspect ratio) at 100 mM DTT converged more rapidly to ~ 1 than those at 75 mM DTT, but with DTT omission, ratios remained at ~ 2 (Figure 2C, D). After coalescence, the relaxation time (m) with varying droplet radii (r) was

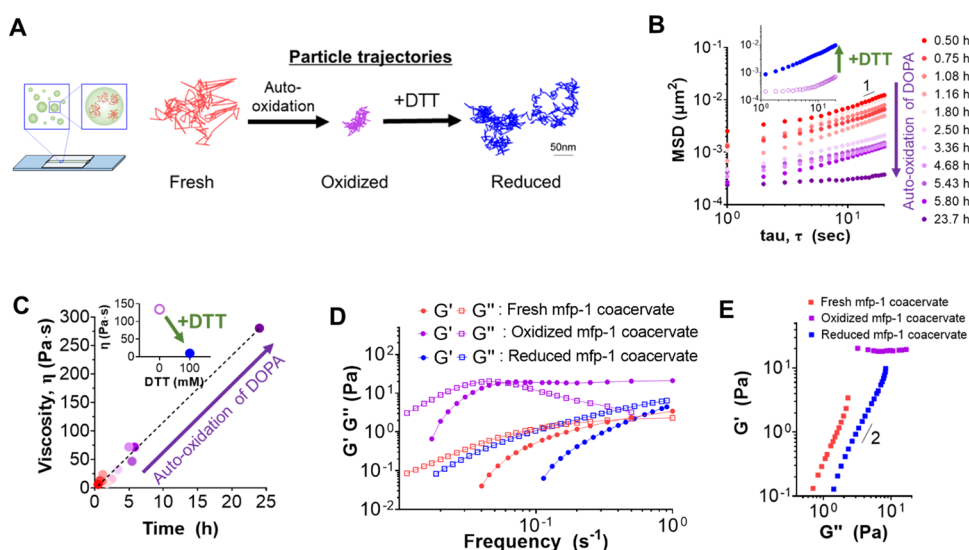


Figure 3. Thiol effects on rheological properties of the like-charged mfp-1 coacervates. (A) Illustration of particle microrheology and particle trajectories in fresh, DOPA-oxidized, and DOPA-reduced coacervate droplets. (B) Mean squared displacement (MSD) of the embedded particles ($n \geq 10$) as a function of lag time (τ) is shown for different DOPA oxidation times. Inset: MSD- τ plots of the oxidized and reduced mfp-1 coacervates by DTT. (C) Viscosity changes of the coacervates depending on DOPA oxidation time. Dashed lines indicate a linear plot. Inset: Viscosity of the oxidized and reduced coacervates. (D) Storage (G') and loss (G'') moduli of the mfp-1 coacervates. (E) Cole–Cole plot. All experiments were carried out at 20 °C.

calculated at 75 mM and 100 mM. Notably, the slope (m/r) from eq 1 was lower at 100 mM than that at 75 mM DTT (Figure 2E), indicating that at 100 mM DTT, the droplets coalesced faster than that at 75 mM because 100 mM DTT restores more DOPA from oxidation products. In the previous studies,^{34,35} DOPA oxidation to quinone and tautomers enhanced adhesion and rigidified the protein backbone. Perhaps, dehydroDOPA and backbone stiffening contribute to the formation of gel-like droplets from mfp-1 coacervates. Figure 2 shows that DTT restores DOPA as well as droplet fluidity, thereby suggesting that thiols are key to maintaining liquidity of mfp-1 coacervates for droplet coalescence.

Effects of Thiols on the Rheological Properties of the Like-Charged Mfp-1 Coacervates. How rheological properties of the like-charged mfp-1 coacervate depend on the DOPA/quinone accumulation were investigated by particle microrheology. A small volume of microparticles (500 nm diameter) was mixed with three types of the like-charged mfp-1 coacervate solutions (fresh, oxidized, and reduced), and the mixed volume was conducted into a channel. The microparticles embedded in the immobile droplets were tracked under a confocal microscope to determine their viscosity and loss/storage moduli (G' and G'') (Figure 3A). The changes in the viscosity of the like-charged mfp-1 coacervates correlated well with the time-dependent DOPA oxidation (Figure 3B,C). As a result, the viscosity increased with incubation time in a roughly linear fashion. The viscosity of the freshly prepared mfp-1 coacervates was 6–12 Pa·s, which significantly increased to a value of 280 Pa·s after 24 h of incubation. Subsequently, the viscosity of the oxidized coacervate droplets was measured both with and without DTT. Surprisingly, the viscosity of the oxidized mfp-1 coacervates decreased from 150 to 10 Pa·s after DTT treatment, which was similar to that of the freshly prepared like-charged mfp-1 coacervates (6–12 Pa·s) (Figure 3B,C).

The loss (G'') and storage moduli (G') versus frequency were also measured to evaluate the viscoelastic behavior of the

coacervates.³⁶ The frequency at which G' and G'' crossover is defined as the beginning of the rubbery plateau region. Fresh like-charged mfp-1 coacervates exhibited a higher crossover frequency (0.42 s^{-1}) than those of oxidized coacervates (0.059 s^{-1}). The crossover frequency was further increased (1.77 s^{-1}) at 100 mM DTT (Figure 3D). In addition, the heterogeneity of DOPA oxidation states in the coacervate droplets was also evaluated by a logarithmic plot of G' versus G'' , namely, a Cole–Cole plot. A linear slope of 2 on the logarithmic plot is empirically associated with shear-thinning behavior in homogeneous polymer solutions.^{43,44} The plot indicates that the fresh like-charged mfp-1 coacervates were homogeneous solutions before DOPA oxidation but became heterogeneous with respect to DOPA oxidation and/or oxidation-dependent conformational changes in mfp-1 (Figure 3E). The homogeneity of coacervates was restored at 100 mM DTT. These striking results support the earlier inference that DOPA residues inside the condensed droplets undergo oxidation to tautomers and quinones and that the gel-like droplets containing the quinone and its tautomers were restored to the liquid-like coacervates by redox exchange with DTT. In addition to viscosity at 100 mM DTT, we estimated interfacial tension of the like-charged mfp-1 coacervate at $\sim 17 \mu\text{N/m}$ from viscosity and eq 1 (Table S1). The low viscosity, low interfacial tension, and low homogeneity represent optimized physical properties for the coalescence-competent like-charged mfp-1 coacervate droplets before metal uptake.

In contrast, DTT had little effect on the rheological properties of recombinant mussel foot protein (Rmfp-1, MW $\sim 14 \text{ kDa}$) coacervates, which do not contain any DOPA. The viscosity and interfacial tension of the Rmfp-1 coacervates unchanged with the addition of 100 mM DTT (Figure S4 and Table S1). This result indicates that the addition of DTT is only effective in the oxidized DOPA-containing coacervates.

In natural cuticle fabrication, mfp-1 coacervate droplets coalesce via their liquid-like behavior prior to metal uptake, as shown by previous studies.^{29,30} However, DOPA oxidation

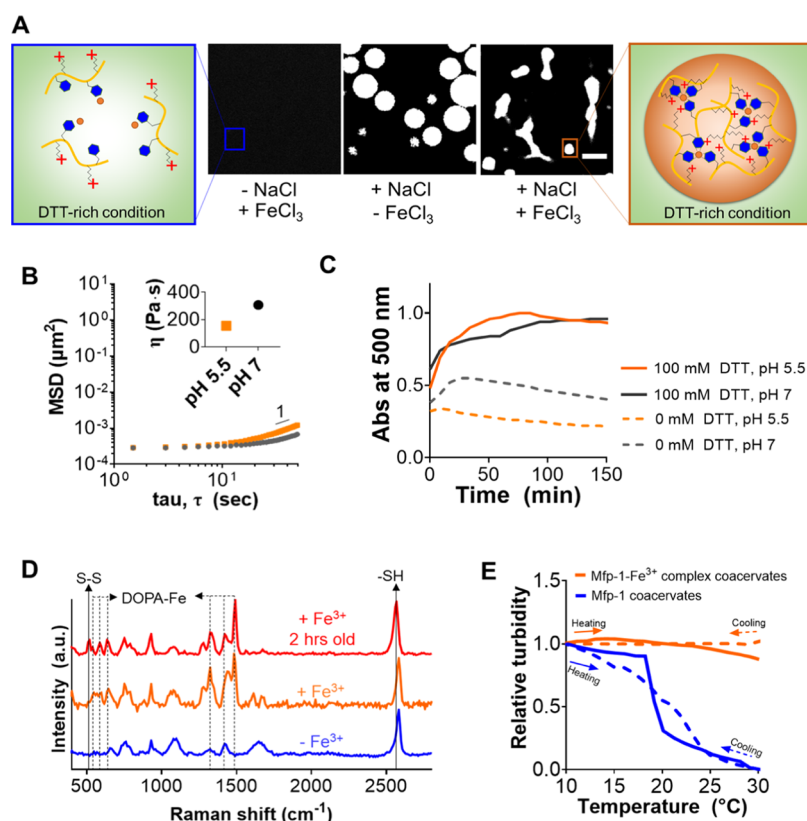


Figure 4. Viscosity and chemical and thermal stabilities of mfp-1-Fe³⁺ complex coacervates under DTT-rich conditions. (A) Formation of mfp-1-Fe³⁺ complex coacervates. Scale bar = 10 μm . (B) Mean squared displacement (MSD) of the embedded particles ($n = 10$) as a function of lag time (τ). Time interval: 1 s. Inset: viscosity at pH 5.5 and pH 7. (C) Relative absorbance of DOPA-Fe³⁺ coordination at 500 nm for 150 min upon the pH and DTT concentrations. Interval: 10 s. (D) Raman spectra acquired from the like-charged mfp-1 coacervates (blue) and the mfp-1-Fe³⁺ complex coacervates (orange and red). Dashed lines indicate Raman peaks of DOPA-Fe³⁺ coordination corresponding to oxygen-metal vibrations (500–700 cm^{-1}) and DOPA ring vibration (1271, 1325, and 1488 cm^{-1}). Solid lines indicate thiol vibration (2564 cm^{-1}) of DTT_{red} and disulfide bond vibration (514 cm^{-1}) of DTT_{ox}. (E) Relative turbidity of the like-charged mfp-1 coacervates (blue) and the mfp-1-Fe³⁺ complex coacervates (orange) measured from 10 to 30 $^{\circ}\text{C}$ at 400 nm under 100 mM DTT condition. Heating (solid line) and cooling (dashed line) rates were 3 $^{\circ}\text{C}/\text{min}$.

dramatically changes rheological properties and hinders the coalescence of mfp-1 droplets. In our study, DTT effectively recovered DOPA from accumulated tautomers and quinones in mfp-1 coacervates as well as inhibiting any further oxidation of DOPA. By these actions, DTT prevented droplet gelation and maintained the liquid-like behavior of the mfp-1 coacervates enabling them to coalesce. We deduce from this that DOPA redox and coacervate fluidity are closely coupled and underline the significance of maintaining a reducing environment during processing.

Conversion of the Mfp-1 Coacervate into Mfp-1-Fe³⁺ Complex Coacervates. Recalling that a critical step of cuticle processing entails recruiting Fe³⁺ into mfp-1 droplets,³⁰ we added 400 μM FeCl₃ to the like-charged mfp-1 coacervates under thiol-rich reducing conditions (Figure 4A). At 400 μM FeCl₃, the molar DOPA to Fe³⁺ ratio was 3:1 in the complex coacervate. By contrast, the treatment of a dissolved mfp-1 solution (low salt) with FeCl₃ formed mfp-1-Fe³⁺ complexes but no microdroplets. According to a previous study,¹⁹ metal-catechol complexation is strongly pH-dependent. Thus, the rheological properties of the mfp-1-Fe³⁺ complex coacervates were evaluated by microrheology at pH 5.5 and 7, where *bis*- and *tris*-catecholato-Fe³⁺ complexes, respectively, predominate. The viscosity at pH 7 (308 Pa·s) was 2-fold higher than that at pH 5.5 (155 Pa·s) and 30-fold higher than those of the

iron-free like-charged mfp-1 coacervates under thiol-rich conditions (Figures 3C, 4B). The crossover frequency at pH 7 was slightly lower than those at pH 5.5 and ~ 16 -fold lower than those of the iron-free like-charged mfp-1 coacervates, indicating that the mfp-1-Fe³⁺ complex coacervates at pH 7 were more elastic (i.e., solid) than either those at pH 5.5 or the iron-free like-charged mfp-1 coacervates (Figure S6).

Earlier, we showed that DOPA in like-charged mfp-1 coacervates was prone to oxidation and that DTT could recover the damage. Thiol and DOPA, however, both bind iron, so knowing whether DTT destabilizes catecholato-iron complexes is critical. Our rheological data showed that the viscoelasticity and coalescence properties altered by the oxidation of DOPA can be restored to that of the fresh mfp-1 coacervates at 100 mM DTT concentration (Figures 2 and 3). Because it was well known that the *tris*-catecholato-iron complex has a maximum absorbance at 500 nm,⁴⁵ it was shown that Fe-DOPA coordination was stable in the presence of DTT over the course of our experiments (Figure 4C). However, the treatment of NaIO₄, which stoichiometrically converts DOPA to DOPAquinone/tautomers, showed no absorbance at 500 nm, indicating that oxidation abolished coordination with Fe³⁺ (Figure S5). In addition, we demonstrated using Raman spectroscopy that the redox activities of DOPA and DTT are coupled in the mfp-1-Fe³⁺ complex coacervates. Freshly

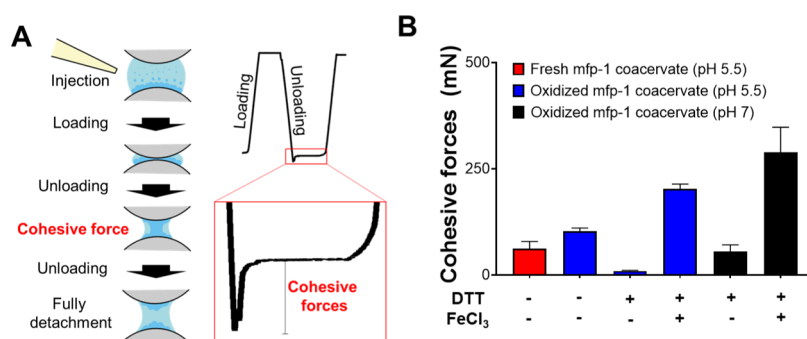


Figure 5. Cohesive forces of the mfp-1 coacervates. (A) Schematic of the SFA experiment for measuring cohesive forces between mfp-1 coacervation. (B) Cohesive forces of the mfp-1 coacervates under different conditions. DTT concentration was 100 mM. FeCl₃ concentration was 400 μ M. All experiments were carried out at 16 $^{\circ}$ C, which is below UCST.

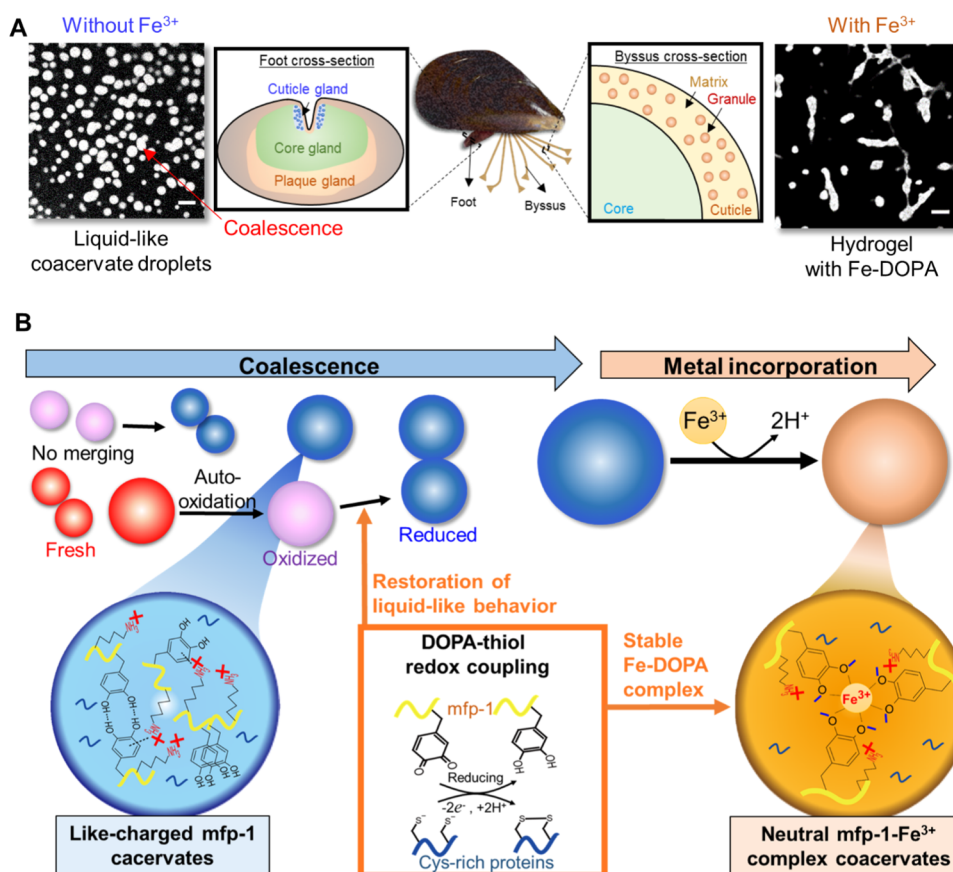


Figure 6. Essential roles of thiols in fabrication of Fe-DOPA complex-containing condensed material. (A) Illustration and confocal microscopic images of mfp-1 coacervates without metal in foot and with metal in the byssal cuticle. (B) Roles of thiols in Fe³⁺-mediated conversion of the liquid-like coacervate droplets into the hydrogels.

prepared mfp-1-Fe³⁺ complex coacervates showed intense Raman peaks at 542, 590, and 639 cm^{-1} (Fe-DOPA interaction) and 1271, 1325, and 1488 cm^{-1} (DOPA ring) (Figure 4D). A thiol peak for DTT also appeared at 2564 cm^{-1} . In addition, a new peak at 512 cm^{-1} , corresponding to the disulfide bond of DTT,⁴⁶ appeared in the complex coacervates after 2 h. The Raman peaks associated with Fe-DOPA complexes remained intense after DTT treatment. Therefore, combining the Raman and UV-vis spectroscopic data, we can infer that the Fe-DOPA complex is maintained by redox exchange with DTT. Although Fe³⁺ and DOPAquinone are both favorable electron acceptors for DTT, apparently only the quinone is reduced.

Finally, we explored the influence of temperature on mfp-1-Fe³⁺ complex coacervates compared with the like-charged mfp-1 coacervates by measuring the turbidity at 400 nm in the range of 10–30 $^{\circ}$ C (Figure 4E). Accordingly, mfp-1-Fe³⁺ complex coacervates did not dissociate in the temperature range. Strong interactions such as metal coordination and electrostatic interaction in the complex coacervates would be expected to endow thermal stability. On the other hand, the like-charged mfp-1 coacervates appeared reversible below 20 $^{\circ}$ C (T_c), which is the upper critical solution temperature (UCST). Other mfps also exhibit the enthalpy-driven UCST behavior.^{47,48} Current thinking is that the UCST behavior originates from the increase of solvent entropy (water) by

strong polymer–polymer interaction.⁴⁹ In the like-charged mfp-1 coacervation, noncovalent interactions such as cation– π interaction (DOPA–Lys) and π – π stacking and hydrogen bond (DOPA–DOPA) are likely to release hydration water molecules from the protein chain, thereby increasing water entropy. In contrast, we found that the recombinant mfp-1 (Rmfp-1) without DOPA has a low critical solution temperature (LCST) behavior (Figure S7). This opposite behavior may arise because, without DOPA, little to no Fe complexation between mfp-1 chains occurs. Therefore, Fe³⁺ incorporation into the like-charged mfp-1 coacervate can provide not only physical changes but also thermal stability.

There is no dispute that metal coordination in the granules of the byssal cuticle achieves viscoelasticity and self-healing behavior in cyclic tension. As a parallel result, the addition of metal to mfp-1 coacervates drastically increases viscoelasticity. However, DOPA instability *in vitro* remains problematic because DOPA seems to be stable in the natural cuticle. Also, the polyphenol network stably coordinates with a specific metal for a long time.¹⁹ These results demonstrate that DTT can provide stability to both DOPA and DOPA–Fe coordination in a mfp-1 condensed phase. This could be chemical evidence of how mussels design their byssus to circumvent DOPA instability.

Cohesive Forces of mfp-1–Fe³⁺ Complex Coacervates.

The cohesive forces of like-charged mfp-1 and mfp-1–Fe³⁺ complex coacervates were evaluated analysis in a surface force apparatus (SFA) (Figure 5A). The measured cohesive forces of the fresh like-charged mfp-1 coacervates were 61.82 ± 17.17 . The oxidation increased the forces to 103.3 ± 7.4 mN (Figure 5B) perhaps because tautomer-dependent chain rigidity of mfp-1 increased. Indeed, the oxidized coacervates in the presence of DTT exhibited low cohesion of 9.7 ± 1.4 mN at pH 5.5 and 55.29 ± 16.02 at pH 7; probably, by reducing the quinone and its tautomers to DOPA, the thiol restored backbone flexibility and fluidity. The dependence of these changes on the accumulation of oxidized DOPA is consistent with the rheological results. Not surprisingly, the addition of Fe³⁺ to the like-charged mfp-1 coacervates with DTT significantly elevated cohesion (199.4 ± 12.1 mN at pH 5.5 and 289.42 ± 58.62 at pH 7), given the formation of Fe–DOPA complexes and enhanced electrostatic adhesion between positively charged lysine and negatively charged Fe–DOPA complex. Diluted mfp-1 (no coacervate) exhibited high cohesive forces with metals but without thiols in previous SFA experiments.^{18,50} This SFA result demonstrates that the mfp-1 coacervates exhibit their highest cohesive forces with FeCl₃ under DTT-reducing conditions. In addition, it suggests that the rheology of mfp-1 coacervates can be toggled up or down depending on the oxidation and metal coordination state of DOPA.

Role of Thiols in Fabrication of Byssal Cuticle. Mfp-1 coacervate droplets are first detected in the phenol gland of foot and, following secretion, undergo coalescence and structural arrest by metal coordination to form the byssal cuticle. Thiol redox has been proposed to explain why DOPA in stable Fe–DOPA complexes is not oxidized in mussels.^{22,24} However, how coupled DOPA–thiol redox impacts the physical properties of the coacervates has not been investigated. Based on our results, we propose two ways by which thiols influence the physical properties of mfp-1 coacervates (Figure 6). Before metal uptake, thiols assure that mfp-1 coacervate droplets maintain their fluidity by inhibiting DOPA oxidation. Such

fluidity enhances the coalescence of coacervate droplets so that the proper dimensions (500 nm diameter) can be achieved in the cuticle. Fluidity also facilitates metal diffusion into the droplets. After metal coordination by DOPA, thiols help maintain stable Fe–DOPA complexation in the mfp-1 coacervate droplets by continuously reducing oxidized DOPA.

CONCLUSIONS

The dense Fe³⁺–DOPA coordination complexes of byssus (particularly in the coating) are critical to its stiffness and good shock-absorbing properties. Although DOPA is easily oxidized in seawater as a free amino acid, mussel-inspired natural strategies for inhibiting DOPA oxidation in byssal proteins have been suspected for some time. In the plaque, for example, DOPA-rich mfp-3 and mfp-5 are coacervated with cysteine-rich mfp-6;^{26,29} likewise, in the cuticle, thiols of mfp-16 to mfp-18 mingle with DOPA-rich mfp-1.²⁷ In both, thiols maintain a reducing poise to prevent DOPA oxidation. Given the pervasive presence of oxygen, however, eventual DOPA oxidation is inevitable. The effect of thiols on the physicochemical properties of mfp-1 following DOPA oxidation has not been previously explored. Our results indicate that thiols restore DOPA from DOPAquinones in the like-charged mfp-1 coacervates resulting in simultaneous restoration of the liquid-like rheological properties that existed prior to oxidation. Iron addition also impacts mfp-1 rheology: Fe³⁺ is rapidly incorporated into the like-charged mfp-1 coacervates resulting in their conversion into hydrogels with drastically increased viscosity and cohesive forces that can be maintained indefinitely in the presence of DTT. Our results suggest that in the byssal cuticle, spherical granules containing dense and reversible catecholato-iron complexes exhibit a durable high energy dissipation under thiol-rich reducing conditions that is lost under oxidizing conditions. In other words, maintaining the reducing redox poise is the price for maintaining a self-repairing and tough byssus in the intertidal region. In addition, thiols, and DTT, more specifically, enable facile processing of Fe³⁺-mediated conversion of liquid-like droplets into hydrogels with improved performance lifetimes based on stable Fe–DOPA complexes. These insights offer much-needed improvements for processing catechol-functionalized polymers in other materials.

ASSOCIATED CONTENT

Supporting Information

The Supporting Information is available free of charge at <https://pubs.acs.org/doi/10.1021/acs.chemmater.2c00406>.

Purification of mfp-1; confocal images of mfp-1 coacervates dependent on NaCl concentration; MALDI-TOF and UV–vis data of mfp-1; microrheology results of Rmfp-1 coacervates; and LCST behavior of Rmfp-1 coacervates (PDF)

AUTHOR INFORMATION

Corresponding Authors

Dong Woog Lee – School of Energy and Chemical Engineering, Ulsan National Institute of Science and Technology (UNIST), Ulsan 44919, Republic of Korea;
orcid.org/0000-0002-1572-9270;
Email: dongwoog.lee@unist.ac.kr

Dongyeop X. Oh – Research Center for Bio-based Chemistry, Korea Research Institute of Chemical Technology (KRICT),

Ulsan 44429, Republic of Korea; orcid.org/0000-0003-3665-405X; Email: dongyeop@kriict.re.kr

J. Herbert Waite – Marine Science Institute, University of California, Santa Barbara, Santa Barbara, California 93106, United States; orcid.org/0000-0003-4683-7386; Email: hwaite@ucsb.edu

Dong Soo Hwang – School of Interdisciplinary Bioscience and Bioengineering, Pohang University of Science and Technology (POSTECH), Pohang 37673, Republic of Korea; orcid.org/0000-0002-2487-2255; Email: dshwang@postech.ac.kr

Authors

Hyungbin Kim – School of Interdisciplinary Bioscience and Bioengineering, Pohang University of Science and Technology (POSTECH), Pohang 37673, Republic of Korea; orcid.org/0000-0002-0312-7256

Jinhoon Lee – School of Energy and Chemical Engineering, Ulsan National Institute of Science and Technology (UNIST), Ulsan 44919, Republic of Korea; orcid.org/0000-0002-8608-027X

Yuri Hong – School of Interdisciplinary Bioscience and Bioengineering, Pohang University of Science and Technology (POSTECH), Pohang 37673, Republic of Korea; orcid.org/0000-0001-9250-8968

Chanoong Lim – School of Energy and Chemical Engineering, Ulsan National Institute of Science and Technology (UNIST), Ulsan 44919, Republic of Korea; orcid.org/0000-0001-6903-0855

Complete contact information is available at:

<https://pubs.acs.org/10.1021/acs.chemmater.2c00406>

Author Contributions

H.K. prepared the samples, performed the experiments, analyzed the data, and wrote the paper. J.L. and C.L. performed and analyzed the SFA measurements. Y.H. prepared Rmfp-1 and conducted the circular dichroism experiments. J.H.W., D.W.L., D.X.O., and D.S.H. advised and directed the project. All authors have given approval to the final version of the manuscript.

Notes

The authors declare no competing financial interest.

ACKNOWLEDGMENTS

The authors thank the support of the Technology Innovation Program (20009508, Development of biodegradation evaluation technology for building circular ecosystem related to bioplastic industry) funded by the Ministry of Trade, Industry, & Energy (MOTIE, Korea), Korea Environment Industry & Technology Institute (KEITI) through Ecological Imitation-based Environmental Pollution Management Technology Development Project funded by Korea Ministry of Environment (MOE) (RE202101305), the National Research Foundation of Korea (NRF) grant funded by the Korea government (MSIT) (No. 2022R1A2C2007874), and the KRICT Core Project (SS2242-10).

REFERENCES

- (1) Petrone, L.; Kumar, A.; Sutanto, C. N.; Patil, N. J.; Kannan, S.; Palaniappan, A.; Amini, S.; Zappone, B.; Verma, C.; Miserez, A. Mussel adhesion is dictated by time-regulated secretion and molecular conformation of mussel adhesive proteins. *Nat. Commun.* **2015**, *6*, No. 8737.
- (2) Waite, J. H.; Vaccaro, E.; Sun, C.; Lucas, J. M. Elastomeric gradients: a hedge against stress concentration in marine holdfasts? *Philos. Trans. R. Soc., B* **2002**, *357*, 143–153.
- (3) Harrington, M. J.; Masic, A.; Holten-Andersen, N.; Waite, J. H.; Fratzl, P. Iron-Clad Fibers: A Metal-Based Biological Strategy for Hard Flexible Coatings. *Science* **2010**, *328*, 216–220.
- (4) Monnier, C. A.; DeMartini, D. G.; Waite, J. H. Intertidal exposure favors the soft-studded armor of adaptive mussel coatings. *Nat. Commun.* **2018**, *9*, No. 3424.
- (5) Harrington, M. J.; Jehle, F.; Priemel, T. Mussel Byssus Structure-Function and Fabrication as Inspiration for Biotechnological Production of Advanced Materials. *Biotechnol. J.* **2018**, *13*, No. 1800133.
- (6) Holten-Andersen, N.; Fantner, G. E.; Hohlbauch, S.; Waite, J. H.; Zok, F. W. Protective coatings on extensible biofibres. *Nat. Mater.* **2007**, *6*, 669–672.
- (7) Holten-Andersen, N.; Zhao, H.; Waite, J. H. Stiff coatings on compliant biofibers: the cuticle of *Mytilus californianus* byssal threads. *Biochemistry* **2009**, *48*, 2752–2759.
- (8) Miserez, A.; Schneberk, T.; Sun, C.; Zok, F. W.; Waite, J. H. The transition from stiff to compliant materials in squid beaks. *Science* **2008**, *319*, 1816–1819.
- (9) Vincent, J. F.; Wegst, U. G. Design and mechanical properties of insect cuticle. *Arthropod Struct. Dev.* **2004**, *33*, 187–199.
- (10) Moses, D. N.; Mattoni, M. A.; Slack, N. L.; Waite, J. H.; Zok, F. W. Role of melanin in mechanical properties of *Glycera* jaws. *Acta Biomater.* **2006**, *2*, 521–530.
- (11) Sever, M. J.; Weisser, J. T.; Monahan, J.; Srinivasan, S.; Wilker, J. J. Metal-mediated cross-linking in the generation of a marine-mussel adhesive. *Angew. Chem., Int. Ed.* **2004**, *43*, 448–450.
- (12) Wilker, J. J. The iron-fortified adhesive system of marine mussels. *Angew. Chem., Int. Ed.* **2010**, *49*, 8076–8078.
- (13) Hwang, D. S.; Waite, J. H. Three intrinsically unstructured mussel adhesive proteins, mfp-1, mfp-2, and mfp-3: analysis by circular dichroism. *Protein Sci.* **2012**, *21*, 1689–1695.
- (14) Sun, C. J.; Waite, J. H. Mapping chemical gradients within and along a fibrous structural tissue, mussel byssal threads. *J. Biol. Chem.* **2005**, *280*, 39332–39336.
- (15) Waite, J. H. Evidence for a repeating 3,4-dihydroxyphenylalanine- and hydroxyproline-containing decapeptide in the adhesive protein of the mussel, *Mytilus edulis* L. *J. Biol. Chem.* **1983**, *258*, 2911–2915.
- (16) Filippidi, E.; Cristiani, T. R.; Eisenbach, C. D.; Waite, J. H.; Israelachvili, J. N.; Ahn, B. K.; Valentine, M. T. Toughening elastomers using mussel-inspired iron-catechol complexes. *Science* **2017**, *358*, 502–505.
- (17) Holten-Andersen, N.; Harrington, M. J.; Birkedal, H.; Lee, B. P.; Messersmith, P. B.; Lee, K. Y.; Waite, J. H. pH-induced metal-ligand cross-links inspired by mussel yield self-healing polymer networks with near-covalent elastic moduli. *Proc. Natl. Acad. Sci. U.S.A.* **2011**, *108*, 2651–2655.
- (18) Zeng, H. B.; Hwang, D. S.; Israelachvili, J. N.; Waite, J. H. Strong reversible Fe³⁺-mediated bridging between dopa-containing protein films in water. *Proc. Natl. Acad. Sci. U.S.A.* **2010**, *107*, 12850–12853.
- (19) Guo, J. L.; Ping, Y.; Ejima, H.; Alt, K.; Meissner, M.; Richardson, J. J.; Yan, Y.; Peter, K.; von Elverfeldt, D.; Hagemeyer, C. E.; Caruso, F. Engineering Multifunctional Capsules through the Assembly of Metal-Phenolic Networks. *Angew. Chem., Int. Edit.* **2014**, *53*, 5546–5551.
- (20) Kim, C. J.; Ercole, F.; Ju, Y.; Pan, S. J.; Chen, J. Q.; Qu, Y.; Quinn, J. F.; Caruso, F. Synthesis of Customizable Macromolecular Conjugates as Building Blocks for Engineering Metal-Phenolic Network Capsules with Tailorable Properties. *Chem. Mater.* **2021**, *33*, 8477–8488.
- (21) Zhou, J. J.; Lin, Z. X.; Penna, M.; Pan, S. J.; Ju, Y.; Li, S. Y.; Han, Y. Y.; Chen, J. Q.; Lin, G.; Richardson, J. J.; Yarovsky, I.; Caruso, F. Particle engineering enabled by polyphenol-mediated supramolecular networks. *Nat. Commun.* **2020**, *11*, No. 4804.

- (22) Miller, D. R.; Spahn, J. E.; Waite, J. H. The staying power of adhesion-associated antioxidant activity in *Mytilus californianus*. *J. R. Soc., Interface* **2015**, *12*, No. 20150614.
- (23) Lee, H.; Scherer, N. F.; Messersmith, P. B. Single-molecule mechanics of mussel adhesion. *Proc. Natl. Acad. Sci. U.S.A.* **2006**, *103*, 12999–13003.
- (24) Yu, J.; Wei, W.; Danner, E.; Ashley, R. K.; Israelachvili, J. N.; Waite, J. H. Mussel protein adhesion depends on interprotein thiol-mediated redox modulation. *Nat. Chem. Biol.* **2011**, *7*, 588–590.
- (25) Wilker, J. J. Biomaterials: Redox and adhesion on the rocks. *Nat. Chem. Biol.* **2011**, *7*, 579–580.
- (26) Valois, E.; Mirshafian, R.; Waite, J. H. Phase-dependent redox insulation in mussel adhesion. *Sci. Adv.* **2020**, *6*, No. eaaz6486.
- (27) Valois, E.; Hoffman, C.; Demartini, D. G.; Waite, J. H. The Thiol-Rich Interlayer in the Shell/Core Architecture of Mussel Byssal Threads. *Langmuir* **2019**, *35*, 15985–15991.
- (28) DeMartini, D. G.; Errico, J. M.; Sjoestroem, S.; Fenster, A.; Waite, J. H. A cohort of new adhesive proteins identified from transcriptomic analysis of mussel foot glands. *J. R. Soc., Interface* **2017**, *14*, No. 20170151.
- (29) Jehle, F.; Macias-Sanchez, E.; Sviben, S.; Fratzl, P.; Bertinetti, L.; Harrington, M. J. Hierarchically-structured metalloprotein composite coatings biofabricated from co-existing condensed liquid phases. *Nat. Commun.* **2020**, *11*, No. 862.
- (30) Priemel, T.; Palia, G.; Forste, F.; Jehle, F.; Sviben, S.; Mantouvalou, I.; Zaslansky, P.; Bertinetti, L.; Harrington, M. J. Microfluidic-like fabrication of metal ion-cured bioadhesives by mussels. *Science* **2021**, *374*, 206–211.
- (31) Ohkawa, K.; Nishida, A.; Yamamoto, H.; Waite, J. H. A glycosylated byssal precursor protein from the green mussel *Perna viridis* with modified dopa side-chains. *Biofouling* **2004**, *20*, 101–115.
- (32) Kim, S.; Huang, J.; Lee, Y.; Dutta, S.; Yoo, H. Y.; Jung, Y. M.; Jho, Y.; Zeng, H.; Hwang, D. S. Complexation and coacervation of like-charged polyelectrolytes inspired by mussels. *Proc. Natl. Acad. Sci. U.S.A.* **2016**, *113*, E847–E853.
- (33) Kim, S.; Yoo, H. Y.; Huang, J.; Lee, Y.; Park, S.; Park, Y.; Jin, S.; Jung, Y. M.; Zeng, H. B.; Hwang, D. S.; Jho, Y. Salt Triggers the Simple Coacervation of an Underwater Adhesive When Cations Meet Aromatic pi Electrons in Seawater. *ACS Nano* **2017**, *11*, 6764–6772.
- (34) Mirshafian, R.; Wei, W.; Israelachvili, J. N.; Waite, J. H. alpha,beta-Dehydro-Dopa: A Hidden Participant in Mussel Adhesion. *Biochemistry* **2016**, *55*, 743–750.
- (35) Yu, J.; Wei, W.; Danner, E.; Israelachvili, J. N.; Waite, J. H. Effects of interfacial redox in mussel adhesive protein films on mica. *Adv. Mater.* **2011**, *23*, 2362–2366.
- (36) Jawerth, L.; Fischer-Friedrich, E.; Saha, S.; Wang, J.; Franzmann, T.; Zhang, X. J.; Sachweh, J.; Ruer, M.; Ijavi, M.; Saha, S.; Mahamid, J.; Hyman, A. A.; Julicher, F. Protein condensates as aging Maxwell fluids. *Science* **2020**, *370*, 1317–1323.
- (37) Mason, T. G.; Ganesan, K.; vanZanten, J. H.; Wirtz, D.; Kuo, S. C. Particle tracking microrheology of complex fluids. *Phys. Rev. Lett.* **1997**, *79*, 3282–3285.
- (38) Leal, L. *Advanced Transport Phenomena: Fluid Mechanics and Convective Transport Processes*, 1st ed.; Cambridge University: New York, NY, USA, 2007.
- (39) Monahan, J.; Wilker, J. J. Cross-linking the protein precursor of marine mussel adhesives: bulk measurements and reagents for curing. *Langmuir* **2004**, *20*, 3724–3729.
- (40) Haemers, S.; Koper, G. J.; Frens, G. Effect of oxidation rate on cross-linking of mussel adhesive proteins. *Biomacromolecules* **2003**, *4*, 632–640.
- (41) Priemel, T.; Palia, R.; Babych, M.; Thibodeaux, C. J.; Bourgault, S.; Harrington, M. J. Compartmentalized processing of catechols during mussel byssus fabrication determines the destiny of DOPA. *Proc. Natl. Acad. Sci. U.S.A.* **2020**, *117*, 7613–7621.
- (42) Shin, Y.; Brangwynne, C. P. Liquid phase condensation in cell physiology and disease. *Science* **2017**, *357*, No. eaaf4382.
- (43) Eom, Y.; Ju, H.; Park, Y.; Chae, D. W.; Jung, Y. M.; Kim, B. C.; Chae, H. G. Effect of dissolution pathways of polyacrylonitrile on the solution homogeneity: Thermodynamic- or kinetic-controlled dissolution. *Polymer* **2020**, *205*, No. 122697.
- (44) Han, C. D.; Kim, J. K. Molecular Theory for the Viscoelasticity of Compatible Polymer Mixtures. 2. Tube Model with Reptation and Constraint Release Contributions. *Macromolecules* **1989**, *22*, 4292–4302.
- (45) Sever, M. J.; Wilker, J. J. Visible absorption spectra of metal-catecholate and metal-tironate complexes. *Dalton Trans.* **2004**, 1061–1072.
- (46) Bazylewski, P.; Divigalpitiya, R.; Fanchini, G. In situ Raman spectroscopy distinguishes between reversible and irreversible thiol modifications in L-cysteine. *Rsc. Adv.* **2017**, *7*, 2964–2970.
- (47) Wei, W.; Tan, Y.; Martinez Rodriguez, N. R.; Yu, J.; Israelachvili, J. N.; Waite, J. H. A mussel-derived one component adhesive coacervate. *Acta Biomater.* **2014**, *10*, 1663–1670.
- (48) Yang, B.; Jin, S.; Park, Y.; Jung, Y. M.; Cha, H. J. Coacervation of Interfacial Adhesive Proteins for Initial Mussel Adhesion to a Wet Surface. *Small* **2018**, *14*, No. e1803377.
- (49) Seuring, J.; Agarwal, S. Polymers with Upper Critical Solution Temperature in Aqueous Solution: Unexpected Properties from Known Building Blocks. *ACS Macro Lett.* **2013**, *2*, 597–600.
- (50) Mesko, M.; Xiang, L.; Bohle, S.; Hwang, D. S.; Zeng, H. B.; Harrington, M. J. Catechol-Vanadium Binding Enhances Cross-Linking and Mechanics of a Mussel Byssus Coating Protein. *Chem. Mater.* **2021**, *33*, 6530–6540.

Recommended by ACS

Tough Antibacterial Metallopolymer Double-Network Hydrogels via Dual Polymerization

JiHyeon Hwang, Chuanbing Tang, *et al.*

JUNE 15, 2022
CHEMISTRY OF MATERIALS

READ 

Photosynthesis of Acetate by *Sporomusa ovata*-CdS Biohybrid System

Ying He, Liang Qiao, *et al.*

MAY 16, 2022
ACS APPLIED MATERIALS & INTERFACES

READ 

Impact of Nanoparticle Size and Surface Chemistry on Peptoid Self-Assembly

Madison Monahan, Brandi M. Cossairt, *et al.*

APRIL 29, 2022
ACS NANO

READ 

Spatial Organization of Photocatalysts and Enzymes on Janus-Type DNA Nanosheets for Efficient CO₂ Conversion

Pegah Tavakoli Fard, Jinheung Kim, *et al.*

JULY 26, 2022
ACS CATALYSIS

READ 

Get More Suggestions >